Modeling and investigation of the performance of a solar-assisted ground-coupled CO_2 heat pump for space and water heating

Thor Alexis Sazon [*], Homam Nikpey

Department of Energy and Petroleum Engineering, University of Stavanger, Kjell Arholms gate 41, Stavanger 4021, Norway

ABSTRACT

The rise in the popularity of heat pumps should be accompanied by the increase in the utilization of environmentally-safe working fluids. To push for wider uptake of hybrid heat pump systems that use natural working fluids, information about their performance and operating characteristics should be made available. This study models a CO_2 solar-assisted ground-coupled heat pump (SAGCHP) system and investigates its performance for space and water heating. Sensitivity analysis, parametric study, and long-term performance simulation were implemented, with the system's seasonal performance factor (SPF), levelized cost of heating (LCOH), and ground temperature change (GTC) considered as performance indicators. It was seen that ensuring a good combination of design and operating specifications can result in an SPF ($\sim$3.5) and LCOH (0.184 USD/kWh) that are comparable with those of SAGCHP systems that use conventional working fluids. The heat pump's high-side pressure and output temperature exhibited notable effects on all the performance indicators. Below the optimal operating pressure, a 5% increase in the heat pump's high-side pressure brought about a $\sim$7–10% improvement to the SPF, a $\sim$3–5% reduction to the LCOH, and a $\sim$6–10% increase to the GTC. Reducing the output temperature by 5% increased the SPF by $\sim$7–8%, decreased the LCOH by $\sim$3%, and increased the GTC by $\sim$6%. Parametric studies identified the presence of optimal heat pump discharge pressure and heat source circulation rate that should be used for operations. Long-term simulation shows that managing the GTC ensures the longevity of the system. Rather than oversizing the borehole heat exchangers (BHEs), it is more practical to reduce ground temperature decline by increasing the BHE spacing or by adding solar collectors.

1. Introduction

The European Union (EU) Strategy for Energy System Integration identifies heat pumps as a key technology for the decarbonization of space heating (SH) and domestic hot water (DHW) production, as well as for cooling in buildings and the industry [1]. In fact, it is already the biggest contributor to the recent increase in renewably-sourced heating and cooling in the EU, accounting for over half of it between 2016 and 2018 [2]. Recent events that have disrupted the supply of gas to Europe indicate that the use of heat pumps is expected to grow further, with a target of 45 million cumulative installations in the residential sector by 2030 [3,4]. Heat pumps can facilitate the utilization of nature's low-grade energy to replace traditional building energy supply with renewable sources and reduce the consumption of high-grade forms of energy, such as electricity and fuels. This helps in reducing the emissions associated with using combustible fuels and contributes to better energy security.

Most heat pumps currently operate through a sub-critical vapor-compression cycle that uses Hydrofluorocarbons (HFCs) as working fluid [5]. HFCs replaced the once widely-used ozone-depleting Chloro-fluorocarbons (CFCs) because they exhibited similarly good performance, efficiency, low toxicity, and non-flammability. However, they were later discovered to be very potent greenhouse gases. For instance, R134a, which is widely used in DHW production, has a global warming potential (GWP) that is 1300 times higher than that of CO_2 [6]. Recent initiatives point out the inevitable phase-down of HFCs. The EU's F-gases regulation (EC517/2014) aims to gradually decrease the usage of important fluorinated gases in the EU, such as R404A, R410A, R407C, and R134a to one-fifth of 2014 in 2030 [7]. Several countries have also committed to cutting their production and consumption of HFCs by more than 80% in the next 30 years under the Kigali amendment to the Montreal Protocol [8].

The combination of using sustainable energy technology with environmentally-safe working fluids is an important notion in the future

---

of the heat pump industry that has revived the interest in natural working fluids. The most widespread natural heat pump working fluids include carbon dioxide, ammonia, butane, isobutane, and propylene [9–11]. Among them, CO_2 (R744) seems to be the most promising, owing to its zero ozone depletion potential, low GWP, non-toxicity, non-flammability, superior thermodynamic properties, and low cost [12–15].

Lorentzen first proposed the modern use of CO_2 in a *trans*-critical heat pump cycle [16]. So far, it has been commercially applied in different sectors, like combined cooling, heating, ventilation, and air conditioning in supermarkets [17,18], water heating [19], and automotive air conditioning [20,21]. Song et al [22] wrote a detailed review of the developments concerning CO_2 heat pump applications. In the *trans*-critical cycle, the high-side pressure and temperature in the supercritical region are not coupled and can be regulated independently to get the optimum operating condition. However, the performance of the *trans*-critical CO_2 heat pump is still generally lower than that of a conventional sub-critical heat pump due to larger irreversibility during expansion, compression, and gas cooling [23,24]. Replacing HFCs with an alternative working fluid requires performances with comparable efficiencies.

One of the ways to improve the efficiency of the heat pump is to introduce changes to its components. The addition of two-phase ejectors to CO_2 heat pump systems has been an important research topic in recent years as a way to recover expansion losses in the thermodynamic cycle [25–30]. Several researchers have seen notable improvements to the performance when the throttle valve was replaced with ejectors. Other studies noted performance improvements from adding a suction gas heat exchanger (SGHX) to the CO_2 heat pump loop [31–36].

Aside from adding or modifying heat pump components, another way to enhance the performance of CO_2 heat pumps is to implement system-wide changes. This can be done by integrating it different energy sources, sizing the system components properly, and by controlling operating parameters to optimize system performance.

Air-source heat pumps (ASHPs) account for the majority of global heat pump sales (60% in 2021) [37]. However, they have the problem of poor low-temperature heating performance and frosting of the heat exchanger [38]. Ground coupled heat pumps (GCHPs) are considered more efficient for indoor climate control applications since they use the heat from the ground, which remains at a nearly constant temperature undisturbed by seasonal weather changes [39,40].

A number of studies have already tackled GCHPs that use CO_2 as their working fluid. Wu et al. [41] developed a 7 kW prototype and a model of a liquid-to-air CO_2 GCHP that could be used investigate performance in residential applications under both sub- and *trans*-critical operations. Wang et al. [42] showed that the performance of a CO_2 GCHP could reach efficiencies similar to an R134a system if it is applied for space conditioning and DHW production, where high water temperature is desired. Bastani et al. [43] performed experiments to investigate the performance of a direct expansion CO_2 GCHP for SH and DHW production. They measured COPs ranging between 2 and 4, depending on its application. Jin et al. [44,45] discussed the application of a CO_2 GCHP for SH, space cooling, and DHW production under warm climate conditions. They showed that the cooling performance of a hybrid CO_2 GCHP system that uses the air and the ground as heat sinks is 42% better than when the air was solely used as the heat sink and 23% better than when the ground is solely used as the heat sink. However, the R410A system still exhibited better annual performance.

The initial installation cost of GCHP systems is typically higher than ASHPs because they require borehole drilling and the installation of borehole heat exchangers (BHE) [39]. Moreover, a single heat source heat pump system is said to be difficult to operate continuously and efficiently [38]. One way to overcome these challenges is to add another heat source, such as solar thermal collectors (SCs). The addition of SCs could allow for shorter BHEs and more operational options.

Studies on solar-assisted ground-coupled heat pump (SAGCHP)

systems that use CO_2 as working fluid is very limited in literature. Kim et al. [23] implemented steady-state simulations to investigate the performance of a CO_2 SAGCHP system under different heat pump operating temperatures, ground temperature, indoor design temperature, and solar radiation. Choi et al. [46] also performed steady-state simulations to compare the performance of a CO_2 and an R22 SAGCHP system under different working fluid inlet temperatures, heat pump operating temperatures, indoor design temperatures, and evaporator inlet temperatures. Note that both studies considered a configuration wherein the SC and GCHP are connected in parallel with a tank thermal energy storage (TTES). Also, relatively low operating temperatures were investigated since the systems were designed for SH applications only.

The reliability of the CO_2 heat pump system requires thorough study since it could exhibit large performance variations with changing operating conditions [23]. To push for wider technology uptake, information about the performance and operating characteristics of the system according to various expected operating and design conditions should be made available.

This paper aims to contribute some knowledge with regard to the design, operations, and performance of CO_2 SAGCHP systems intended for SH and DHW production. Compared to the available literature, our study investigates a different system configuration and focuses on a different application. We also implemented a more practical approach to investigating the system. Most of the parameters considered here include those that could easily be adjusted during the design and operating stage. Both efficiency and cost were considered as performance indicators, and they were calculated while considering seasonal variations in weather and demand. This gives insights into the achievable system performance given realistic variations in boundary conditions.

2. Methods

The thermal system model was developed using Modelica through the Dymola v2021x [47] graphical user interface (GUI). It includes a CO_2 heat pump, glazed flat plate SC, BHEs, a TTES, and SH and DHW demand information. The CO_2 heat pump was modeled using the Thermal Systems library v1.6.1 [48] and then calibrated with experimental data; the BHEs were modeled using a modified version of the MoBTES library v2.0 [49]; the SCs and TTES were both modeled with the Buildings library v9.0.0 [50]. Modelica Standard Library (MSL) v4.0.0 was used in this study. Simulations that span a year were run to capture seasonal variations in some parameters and boundary conditions. The performance indicators investigated include the seasonal performance factor (SPF), the levelized cost of heating (LCOH), and the ground temperature change (GTC) induced by the system. The effects of varying the values of selected design and operation parameters to the performance indicators were determined and analyzed.

2.1. Development of the thermal system model

Shown in Fig. 1 is the schematic of the thermal system model in the Dymola GUI. As shown, the SCs and the BHEs were connected in series and provide the low-temperature heat input to the CO_2 heat pump's evaporator. There are studies that have compared different configurations/operations of hybrid solar-geothermal HP systems, but they all seem to have focused on conventional subcritical HPs. Some studies have favored the BHEs and SCs to be connected in series [51–53]. Other studies favored the BHEs and SCs to be connected in parallel [54,55].

The series configuration was arbitrarily chosen for this study since it theoretically allows the storage of excess solar energy into the ground and helps in managing the thermal imbalance induced by utilization. When solar irradiation is available, the SC heats up the cold water-side fluid coming from the evaporator of the heat pump. The solar-heated fluid is then directed to the BHEs, where it either extracts or injects
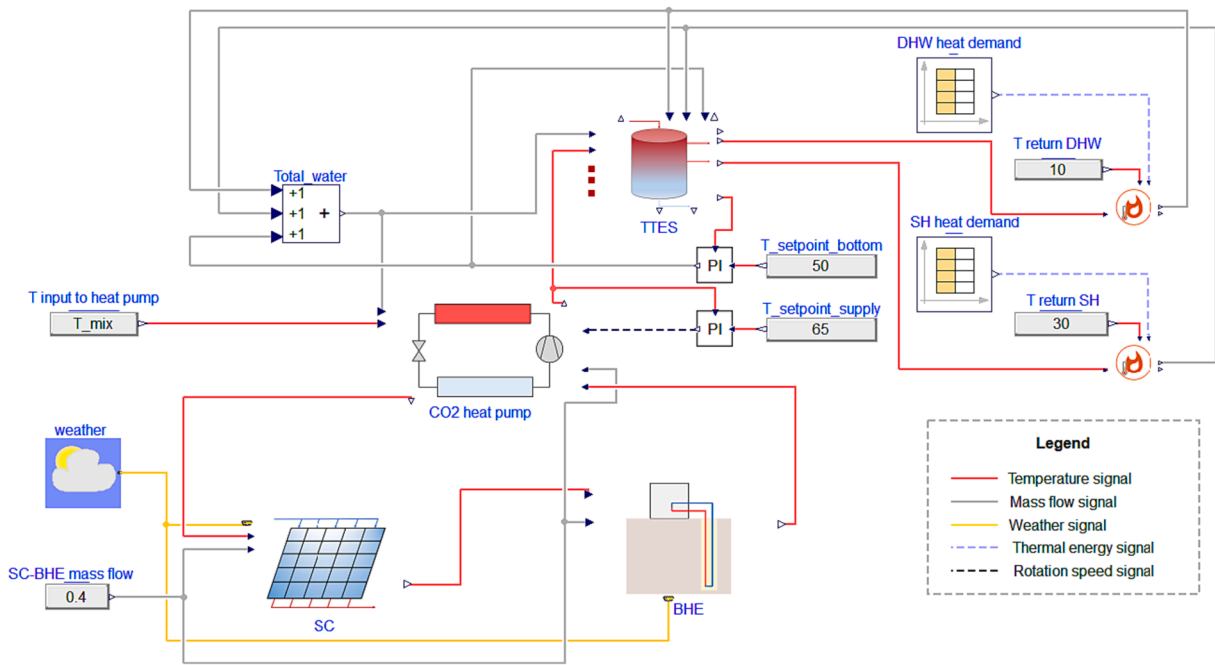
Fig. 1. The thermal system model.

energy, depending on its temperature relative to the ground. Through the BHEs, the ground could function as both a heat source and heat storage. After the BHEs, the fluid then goes to the CO_2 heat pump, where it delivers the heat needed to evaporate the CO_2 working fluid. The base value of the mass flow of the fluid circulating through the SC, the BHE, and the water side of the heat pump's evaporator (0.42 kg/s) was estimated using the American Society of Heating, Refrigerating and Air-Conditioning Engineers (ASHRAE) methodology [56]. The weather of Bergen, Norway, obtained from the EnergyPlus database [57], was used in this work.

A controller that varies the rotational speed of the compressor is used to set the supply temperature of the CO_2 heat pump (base value of 65 °C). Another controller manages the flow from the bottom of the

TTES to ensure that the temperature there does not go below 50 °C. This ensures that the temperature in the DHW distribution system is kept higher than the proliferation temperature of Legionella (20——45 °C) [58].

Although not explicitly modeled here, the heat for SH and DHW heating was assumed to be provided through a heat exchange process with the distribution system. While Legionella proliferation is not a problem for this specific system since DHW is supplied using running water heated through a heat exchanger, we considered temperature levels that keeps this risk at bay in consideration for other systems that are not designed similarly.

Hot water from the top and from the middle to the TTES is withdrawn to provide the energy required for DHW production and SH,
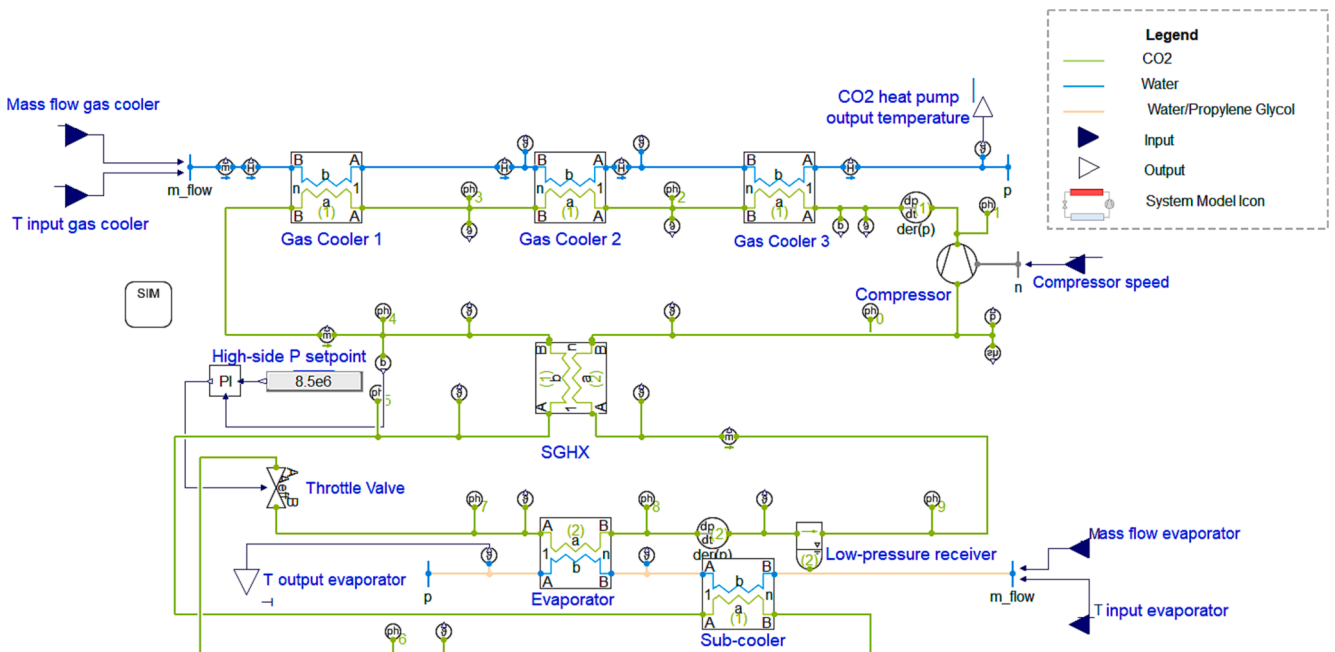

Fig. 2. The CO_2 heat pump component model.

respectively. The colder fluid used for SH, DHW heating, and from the bottom of the TTES all gets recirculated, mixed, and then reheated in the heat pump. The temperature of the fluid after being used for DHW production was set at 10 °C. Since the city water was assumed to be at 7 °C, this assumes that the heat exchange process for DHW production occurred at a 3 °C pinch temperature. The SH return temperature was given a base value of 32 °C but was varied as one of the control parameters. The demand side was represented by hourly thermal demand data.

2.1.1. Modeling of the CO₂ heat pump

The CO_2 heat pump model (Fig. 2) was based on a 6.5 kW prototype unit constructed and tested by Stene [59,60]. It consists of the counter-flow tripartite gas coolers, an evaporator, a compressor, a throttle valve, an SGHX, a sub-cooler, and a low-pressure receiver.

The throttle valve and the low-pressure receiver function together to control the high-side pressure of the heat pump [59]. Reducing the valve opening accumulates more CO_2 in the gas cooler piping and increases the high-side pressure; opening the valve reduces it. The CO_2 is stored or boiled off from the receiver as needed.

Measured data for the design condition at 8.5 MPa were used to calibrate the model. The information available in Stene's work [59] was used to specify the values of some parameters in the model, including the tube diameters of all the tube-in-tube heat exchangers, their weights, material of construction, and length; the size of the low-pressure receiver; and the compressor displacement and operating range. The parameters adjusted during calibration include: (a) the coefficient of heat transfer in each heat exchanger and (b) the isentropic and overall efficiencies of the compressor. A compressor model with fixed efficiencies was utilized for simplicity.

2.1.2. Modeling of the borehole heat exchangers

Fig. 3 shows the BHE model developed with the MoBTES library [49]. The MoBTES library, a free and open Modelica library that is comprised of tested and validated components for the simulation of BHEs, was originally developed under MSL v3.4. In this work, the library was revised to function with MSL v4.0. The most recent version of MoBTES is now integrated into the solar district heating library MoSDH [61,62].

The parameters assumed to calculate the size of the BHE, using the ASHRAE methodology, are given in Table 1. It was assumed that 4 BHEs are needed to provide the ~6.5–7 kW heat required by the demand. The ground was assumed to have the characteristics of Slate, one of the common rock types in some parts of Norway [63] while the thermal gradient was assumed to be 0.0125 K/m, similar to some wells drilled in Bergen, Norway [64]. Following the procedure in the ASHRAE method, a borehole length of 80 m/well and a circulating fluid mass flow rate of 0.42 kg/s were calculated. These were used as the base values for the

Fig. 3. The BHE component model.

Table 1
Summary of BHE parameters.

BHE parameter	Value
Geothermal gradient, K/m	0.0125
Ground density, kg/m³	2760
Ground specific heat, J/kg-K	920
Ground thermal conductivity, W/m-K	2.1
Layout	Rectangle
BHE type	Single U
Number of BHEs	4
Borehole diameter, m	0.15
Tube inner diameter, m	0.034
Tube thickness, m	0.003
Tube thermal conductivity, W/m-K	0.4
Shank spacing, m	0.08
Number of BHE in series	1
Grout density, kg/m³	1900
Grout thermal capacity, J/kg-K	1300
Grout thermal conductivity, W/m-K	1.5
BHE length base value, m/well	80

analysis.

This BHE model connects with the heat pump model and to the SC model through the outlet and inlet temperature signals, respectively. The BHE is connected in series with the SC and the heat pump, hence the mass flow rate through all of them is the same.

2.1.3. Modeling of the solar thermal collectors

The solar model (Fig. 4) was developed using the Buildings library v9.0.0 [50]. The Buildings library is a free and open-source Modelica library that comprises of tested and validated components for the simulation of buildings, district heating, and control systems. The main components of the solar thermal model in this work are the solar pump controller and the solar thermal collector.

The solar pump controller dictates whether the pump to the SCs is active or inactive depending on the value of the incident solar radiation and system parameters. The pump is activated when the incident solar radiation is higher than the critical radiation, defined by Eq. (1) in Duffie and Beckman [65].

$$G_{TC} = (F_R U_L (T_{in} - T_{ENV}))/(F_R(\tau\alpha)) \tag{1}$$

Where G_{TC} is the critical solar radiation, $F_R U_L$ is the heat loss coefficient, T_{in} is the inlet temperature, T_{ENV} is the ambient temperature, and $F_R(\tau\alpha)$ is the maximum efficiency. The solar collector was modeled according to the EN12975 test standard [66]. EN 12975 test data for a glazed flat-plate solar collector (WTS-F1-K1/K2 from Max Weishaupt GmbH) was utilized in this study [67]. Given in Table 2 are the SC parameters used in the model.

When the incident solar radiation is lower than the critical radiation, the fluid bypasses the SCs and goes directly to the BHE. The solar thermal model is connected to the CO_2 heat pump and BHE models by temperature signals.

2.1.4. Modeling of the tank thermal energy storage

The model for the TTES (Fig. 5.) was also developed using components of the Buildings library. The model uses the stratified storage tank model, which implements several volumes that exchange heat among themselves and with the ambient via conduction. Each layer volume contains a fluid port that may be used to inject or withdraw water to or from the tank. Heat loss through the top and sides of the TTES was modeled by assuming that the ambient temperature is kept at 19 °C, the minimum acceptable indoor temperature according to Norwegian building regulations [68]. Insulation thickness and conductivity were assumed to be 200 mm and 0.04 W/m-K, respectively. The TTES height was kept at 2 m. Hot fluid from the heat pump first passes through a backup heater in case the required temperature was not attained. It is then injected into the top layer of the tank. Relatively cold fluid is drawn
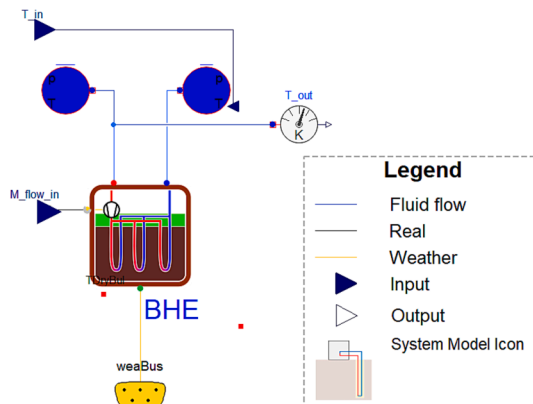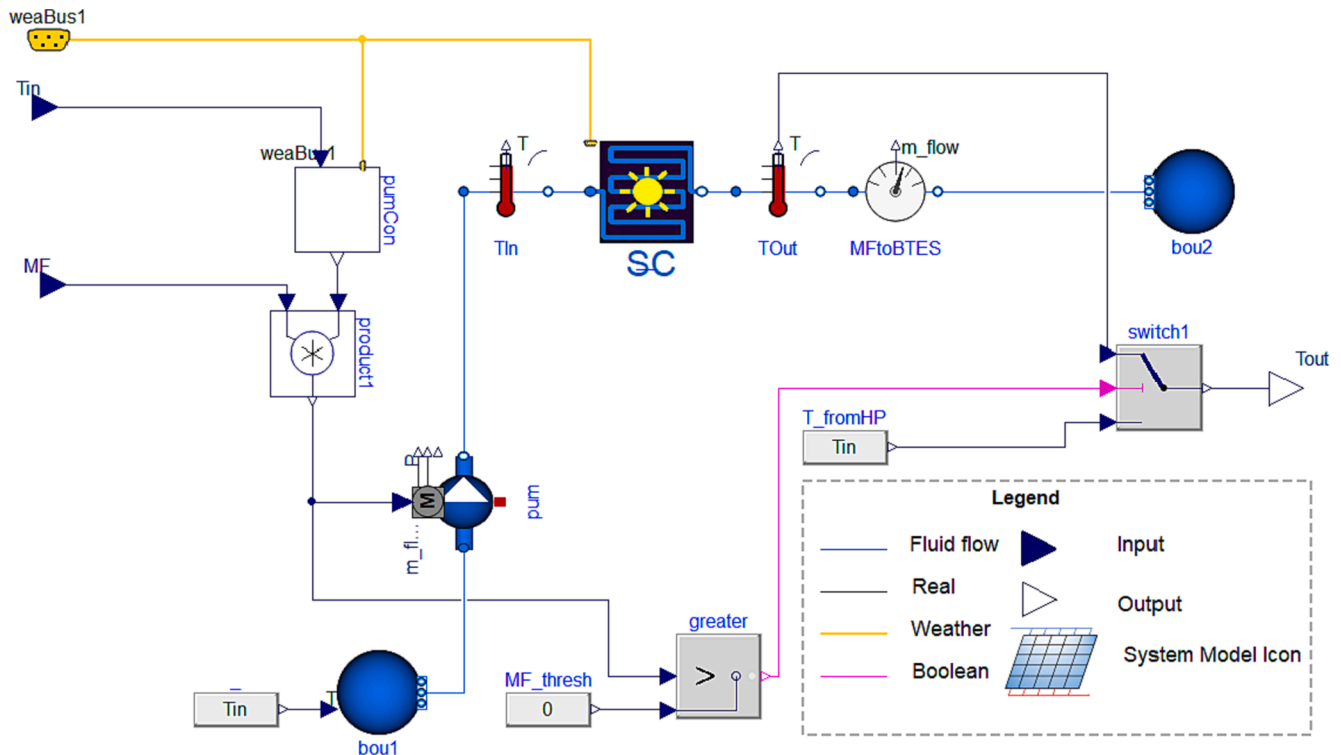
Fig. 4. The solar thermal component model.

Table 2
Summary of SC parameters following the EN 12975 test standard [67].

SC parameter	Value
Area/collector, m^2	2.32
Dry weight, kg	42
Fluid volume, m^3	0.0023
Pressure drop during test conditions, Pa	100
Mass flow per unit collector area, kg/s-m^2	0.02
Maximum efficiency	0.802
Heat loss coefficient	3.601
Temperature dependence of heat loss	0.014
Incidence angle modifier	0.97
Nominal solar irradiance in ratings data, W/m^2	1000
Nominal temperature difference in ratings data, K	20

from the bottom to manage the temperature inside the tank. Hot water from the top and the middle layers are withdrawn to provide the energy required for DHW heating and SH, respectively. The rate of withdrawal of water is controlled by the thermal demand model component.

2.1.5. Model of the thermal demand

Thermal energy demand (Fig. 6) was represented by a pipe, which features a heat port. The heat port is connected to demand information, which could either be obtained from measurements or simulations. The flow of hot fluid coming from the TTES is controlled by indicating the expected temperature of the fluid after it has undergone heat exchange with the distribution system. This model is a simplification of how the heat demand is being met by the system.

Hourly demand data for space and water heating from a school in Stavanger, Norway was utilized as the reference of the demand input to this model. The choice of using heat demand and weather data from two different cities was limited by the data availability. Nonetheless, Stavanger and Bergen are two cities close to one another, that have relatively similar climate conditions. The capacity of the system model in this study is limited to 6.5 kW since the data used to calibrate the CO_2 heat pump is from a 6.5–7 kW prototype unit. The demand data from the

school is much higher than this so it was normalized, by dividing all data by the measured maximum demand, and then multiplied to 3 kW and 3.5 kW for space and water heating, respectively (Fig. 7). Peak demands, which comprise less than 1% of the total demand data, were also filtered out for simplicity. Hence, the actual magnitude of the energy demand from the school was not used but the demand patterns were followed. Space heating goes up in the winter and during school hours and goes down in the summer. Water heating more or less retains its level throughout the year. Typical demand profiles on a weekday for the different seasons are also given in Fig. 7. The demand profiles in spring and autumn are fairly similar; the demand in summer is considerably smaller; winter demand is the highest among all of them.

2.2. The performance indicators

The system performance indicators chosen for this study are the SPF, the LCOH, and the GTC. Due to the complexity of the model, simulation runs require substantial amounts of time to finish. Since the study requires running several cases, it was decided to limit the simulation time for the sensitivity and parametric studies to 1 year. Of course, more representative values of the performance indicators could have been obtained if the simulations covered the whole lifetime of the system. A trial run showed that the SPF and LCOH did not vary so much yearly. On the other hand, the GTC was highest for the first year but substantially decreased in the succeeding years. This was assuming that the weather and the demand remained consistent yearly.

To calculate the SPF, the total energy delivered by the system to the demand was divided by the total energy utilized to run the system. The SPF pertains to the system and not only the heat pump. Energy utilization includes the total annual electricity used to run the compressors and the circulation pumps. A higher SPF indicates better efficiency.

To calculate the LCOH, the operations cost and thermal energy delivered from a year of simulation were first assumed to be the yearly operations cost and energy generation of the system. The assumed cost annuity was then discounted back to its present value using the discount rate (r) and added to the total capital cost of the system. The sum was
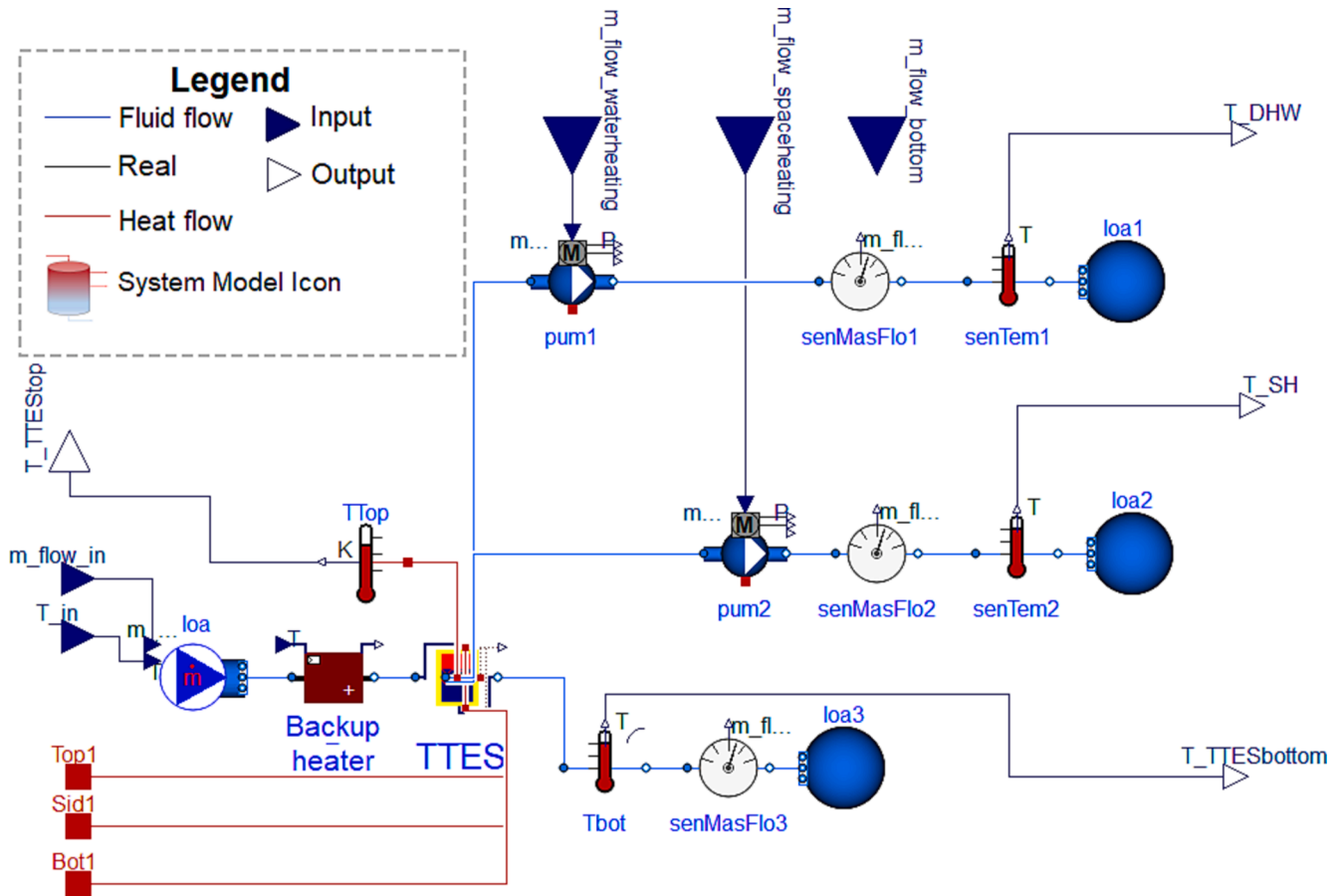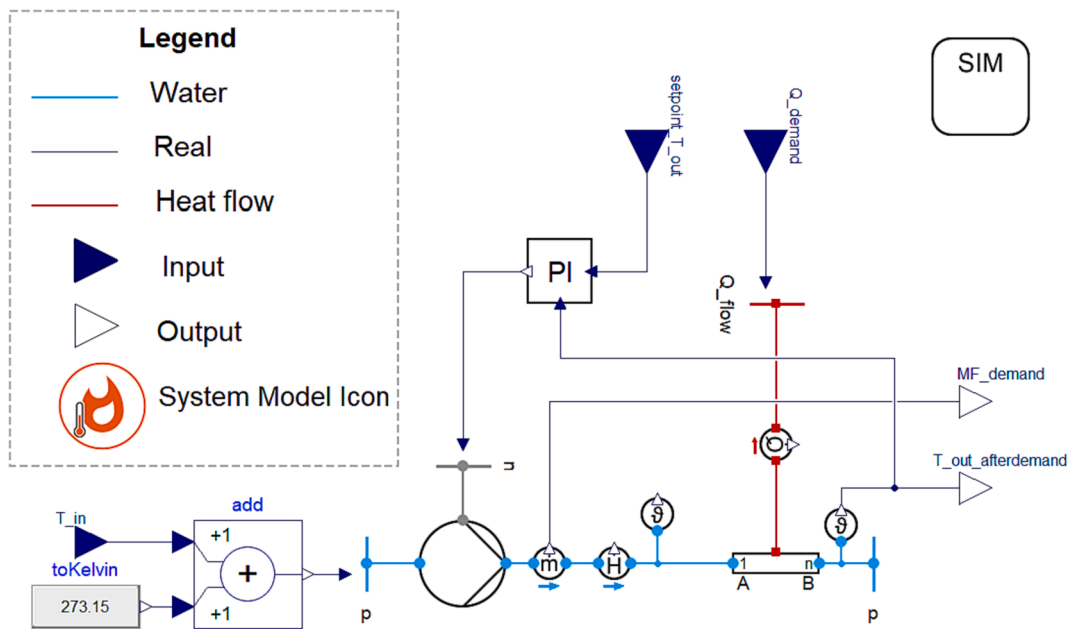
Fig. 5. The TTES component model.

Fig. 6. The thermal demand component model.

then divided by the discounted value of energy generation.

$$LCOH = \frac{A\left[\frac{1-(1+r)^{-n}}{r}\right] + C}{E\left[\frac{1-(1+r)^{-n}}{r}\right]}$$

(2)

Where A is the annual cost of operations, r is the discount rate, n is the lifetime of the system, C is the capital cost, E is the yearly energy generation of the system.

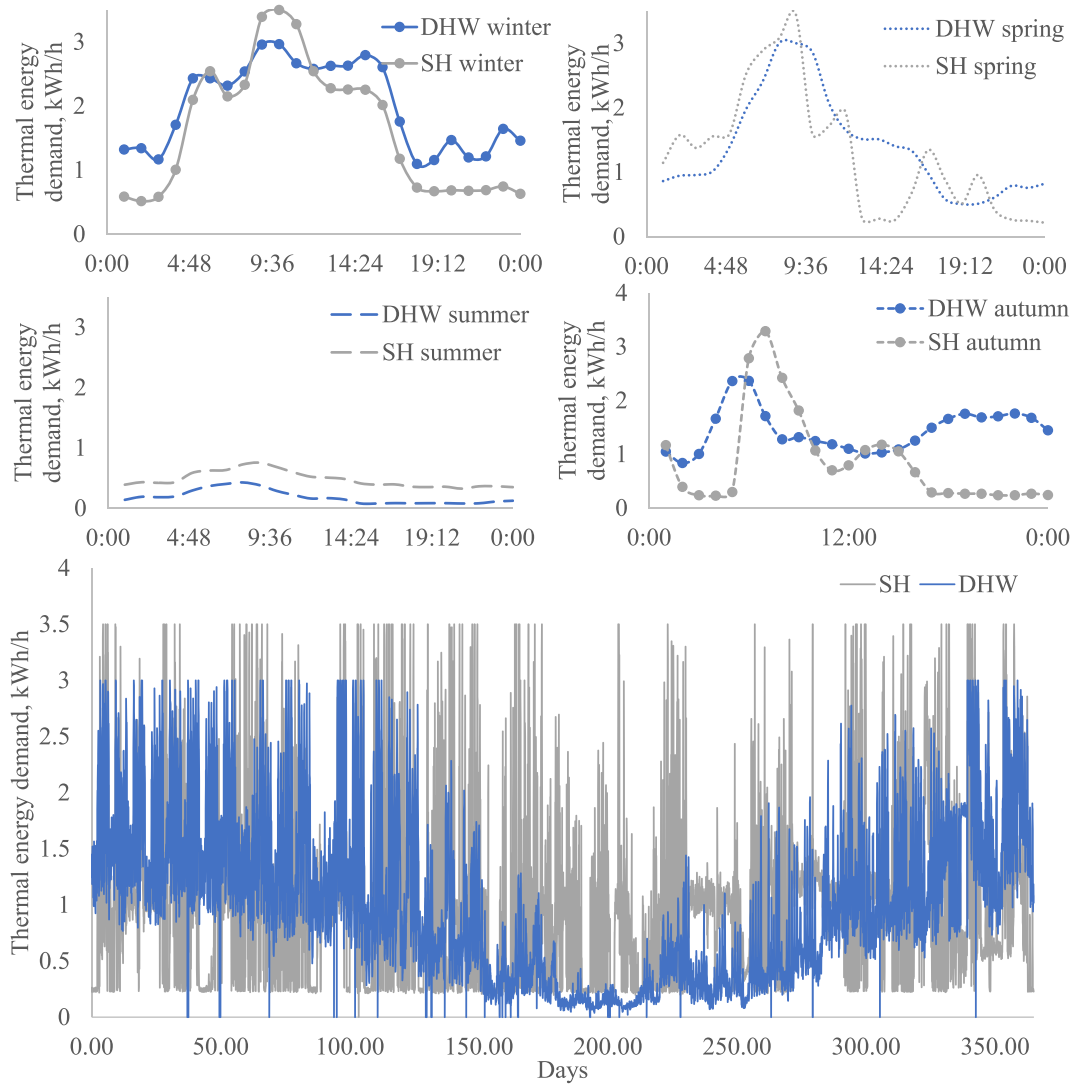The LCOH signifies the cost of producing 1 kWh of heating, and it is

Fig. 7. The thermal demand for a year and for typical days in different seasons.

affected by both the cost of the equipment and the efficiency of

Table 3
Summary of parameters used for cost calculations.

Parameter	Value	Reference/Notes
Cost of flat plate SC, EUR/ m²	632.5	Average of SC costs in [69]
Cost of BHE, EUR/m²	65	[70]
Cost of TTES, EUR/m³	1150	Average cost of 0.8 – 2 m³ TTES [71]
CO_2 Heat pump compressor cost, CNY	17547 $W^{0.4488}$	W is the rated compressor power [72]
CO_2 Heat pump gas cooler cost, CNY	1874.4$A^{0.9835}$	A is heat exchanger area [72]
CO_2 Heat pump evaporator cost, CNY	331.7$A^{0.9390}$	A is heat exchanger area [72]
Lifetime of system, years	25	[70,73]
Discount rate	2%	Discount rate or cost of capital for heat pumps [74]
Exchange rate, USD/€	1/1.01	Exchange rate in Sept. 2022
Exchange rate, USD/CNY	0.14/1	Exchange rate in Sept. 2022
Exchange rate, NOK/USD	1/0.0975	Exchange rate in Sept. 2022
Electricity cost, NOK/kWh	2.4415	Average electricity price in Norway in 2022 [75]

EUR = Euros; CNY = Chinese Yuan; USD = U.S. Dollars; NOK = Norwegian Kroner.

operations. A lower LCOH is desired. The data and assumptions used for cost calculations are summarized in Table 3.

The GTC was obtained from the BHE model. The model gives out the average ground temperature as it is utilized as a heat source or sink. GTC is calculated by subtracting the ground temperature after one year of simulation from the initial ground temperature ($T_{initial} - T_{final}$). When consistent boundary conditions are applied to a SAGCHP system, GTC is expected to reduce after the first year since the driving force for heat exchange between the circulating fluid and the ground gets smaller. In this study, the 1st-year GTCs calculated in the sensitivity and parametric runs were assumed to represent the maximum expected temperature decline for a year of operation. A higher GTC value means a larger ground temperature decrease. A negative GTC pertains to the accumulation of heat in the ground. A GTC close to zero or slightly negative is desired.

2.3. The sensitivity, parametric, and long-term performance studies

The effects of varying the value of selected parameters to the performance indicators were investigated in this study. A total of 8 parameters (Table 4) were varied, 4 pertain to design conditions while the other 4 to operating conditions. The BHE length, SC area, and TTES volume were chosen since they are known to have a direct relationship with the cost of the system. The SC-BHE mass flow, CO_2 heat pump high-

Table 4
Parameters investigated.

Parameter	Base Value	Range of variation (Parameter investigation)
BHE length, m	80	50 – 200
BHE spacing, m	5	3 – 8
SC area, m^2 (number of collectors)	13.92 (6)	4.64 – 23.2 (2 – 10 collectors)
TTES volume, m^3	1	0.3 – 3
SC-BHE mass flow, kg/s*	0.42	0.05 – 1
SH return temperature, °C	32	20 – 40
CO$_2$ heat pump high-side pressure, MPa	9	8.5 – 10
CO$_2$ heat pump output temperature, °C**	65	60 – 75

*the flow rate of the fluid circulating through the SC, BHE, and the evaporator's water side.

**the temperature of the water as it comes out of the water side of the gas cooler before entering the TTES.

side pressure, and heat pump output temperatures were chosen since they are parameters that could easily be controlled. The BHE spacing was also included since it could be a non-expensive way to diffuse the thermal imbalance induced by the system to the ground. Lastly, the return temperature was included to indirectly represent the effects of the performance of the distribution system on the energy supply system.

A sensitivity study was first implemented by individually changing the base value of the parameters by ± 5% and observing how a similar magnitude of change induced to each of them affects the performance indicators. The induced parameter variation in the sensitivity runs was limited to ± 5% because there is a limit on how low the high-side pressure of the heat pump could be changed.

Since it is expected that this system would not respond linearly to every parameter, a wider range of values must be investigated. The result of this parametric study was then analyzed to discuss the trade-offs among different parameter specifications in terms of performance and cost. Table 4 shows the base value of the parameters and the range of variation implemented in the parametric study.

From the results of the parametric and sensitivity runs, a combination of parameter values that would allow the system to perform well was chosen and used for a long-term simulation run. Due to the limitations of data availability, the demand used for the first year of simulation was reused in the subsequent years. The simulation time was limited to 10 years because of the relatively large amount of time needed to run the model.

3. Results and discussion

The CO$_2$ heat pump was first calibrated using measured data [59]. Other component models were validated as well. After this, sensitivity and parametric studies were implemented. Lastly, a long-term simulation run was implemented using a combination of parameter values that were deemed to give favorable performance.

3.1. Calibration or validation of component models

The best way to verify the validity of a system model is to calibrate it against data from a real-world installation of the exact system. However, since neither the facility nor data are available to the researchers, some of the components were just calibrated or validated individually. The SC implements a widely-used standard model whose validation is included in the Buildings library [50]. It was decided not to re-validate it here. The MoBTES library is relatively new and was slightly revised in this work so re-validation was implemented to see how it performs on other data different from what the developers used. The TTES was also validated here since its validation model was not included in the Buildings library. The heat pump was modeled using more basic components, such

as heat exchangers, valves, and compressors. Hence, it required calibration.

3.1.1. Calibration of the heat pump

Available data [59] was used for the calibration of the heat pump. The measured data for the design condition at 85 bars were used to calibrate the model. Some component specifications were obtained from the reference material while some were determined through the calibration process. During the calibration, the values of the heat transfer coefficients of every heat exchanger and the efficiencies of the compressor were adjusted until the model could simulate measured test data. Table 5 shows the values of the heat exchanger parameters while Table 6 shows the parameters for the other heat pump components, such as the low-pressure receiver and the compressor.

Table 7 gives the results of the CO$_2$ heat pump calibration runs. The model was calibrated against the data for the high-side pressure P$_{GC}$ = 85 bars, while the other measured data were used to test the calibrated model. Calibration and test errors were obtained by comparing the measured and simulated COPs. As shown, the error generated by the calibrated model increases when it is used to simulate the off-design lower high-side pressure. This can be partly attributed to the choice of using a simplified compressor model that assumes constant efficiencies. Nonetheless, the simulations performed in this work use a lower limit of 85 bars, thus avoiding the larger errors associated with the 80 bars.

3.1.2. Validation of the BHE

The BHE model was validated using data from a seasonal thermal energy storage facility in Neckarsul, Germany [76]. The facility was built in 1997 and consists of 36 double U-tube BHEs with a depth of 30 m. Given in Table 8 are the specifications of the BHEs. Neckarsulm, Germany [76].

Operation data from January 1 to March 1, 1998, were used to assess the accuracy of the model. The measured and simulated outlet temperatures from the BHEs are compared in Fig. 8. The boundary conditions used include the inlet temperature, which varied between 50 and 80 °C, and the volumetric flow rate, which remained at around 0.0034 m^3/s. It was observed to accurately predict the outlet temperature of the fluid after passing through the BHEs. A small root-mean square error (RMSE) of 2.24 was calculated, signifying that the model could sufficiently simulate the behavior of the real system.

3.1.3. Validation of the TTES

The TTES model was validated using data from an experimental facility that incorporates a 785 l Wolf BSP-800 TES tank [77]. Eight (8) temperature sensors can be found throughout the active section of the tank, thereby subdividing it into 8 layers. A multi-node stratified TTES model with a height of 1755 mm and diameter of 790 mm was used to represent the active layers of the tank. Each tank layer was represented by 5 nodes, resulting in a 40-node TTES model. When comparing the results to measured data, the simulated temperatures from the 5 nodes that represent a layer were averaged. The amount of heat loss was not given in the paper, so it was assumed to occur at the top and sides of the TTES, given the ambient temperature of 20 °C, an insulation thickness of 150 mm, and an insulation thermal conductivity of 0.05 W/m-K. During the experiment, the tank was charged for 3 h from a fully discharged condition (state of charge (SoC) = 0%), increasing the storage temperature from 20 °C to 60 °C. It was then discharged for the next 2 h. During discharge, the temperature of the fluid entering the tank's bottom was kept at around 30 °C, representing the return temperature from domestic heating systems. The charging and discharging temperature and flow rates (Fig. 9) were used as inputs to the TTES model.

The resulting simulated temperatures for every layer and the SoC were then compared to the measured ones in Fig. 10. The SoC was taken by taking note that the maximum and minimum operating temperatures of the tank are 85 °C and 20 °C, respectively (Eq. (3).

Table 5

CO$_2$ heat pump heat exchanger specifications.

	Gas Cooler 1	Gas Cooler 2	Gas Cooler 3	Evaporator	Sub-cooler	SGHX
CO$_2$-side tube length, m	14	15	3.5	12	6	2.3
CO$_2$-side tube inner diameter, m	0.006	0.006	0.006	0.008	0.008	0.08/0.12
CO$_2$-side heat transfer coefficient, W/m^2-K*	9000	7000	3500	6500	150	550
Water-side tube length, m	14	15	3.5	12	1	NA
Water-side tube inner diameter, m	0.012	0.018	0.012	0.02	0.025	NA
Water-side heat transfer coefficient, W/m^2-K*	9000	7000	5500	4500	150	NA
Wall thermal resistance, K/W (Stainless Steel)	0.00025	0.00025	0.00025	0.00025	0.0001538	0.00025
Mass, kg	13	18	6	17	17	2.5

*Values determined from the calibration process.

Table 6

Other CO$_2$ heat pump component specifications.

Component	Parameter	Value
Compressor (Hermetic two-stage rolling piston unit operated as a single-stage unit)	Operating speed, rpm (Hz)	1800–7200 (39–120)
	Displacement, cm^3/rev	3.33
	Swept volume, m^3/h	1.439 at 7200 rpm
	Volumetric Efficiency*	0.85
	Isentropic Efficiency	0.8
	Effective Isentropic Efficiency*	0.62
	Max discharge temperature, °C	125
	Max power input, W	2500
Evaporator	Evaporation temperature, °C	−5
	Mean temperature difference, K	~5
Tripartite gas coolers	SH heating capacity, kW	~3
	SH temperature approach, K	<0.2
	DHW - Water temperatures, °C	5/60
	DHW - Heating capacity, kW	~3.5
	DHW - Temperature approach, K	<3
Low pressure receiver	Volume, m^3	0.004
	Initial filling level	0.5
Throttle valve	Effective flow area, m^2	$1 \times 10^{-8} - 3 \times 10^{-7}$

*Values determined from the calibration process.

$$SOC = \frac{\left(\sum_{i=1}^{N} c_{p_i} \rho_i V_i T_i\right) - c_{p_{min}} \rho_{min} V T_{min}}{c_{p_{max}} \rho_{max} V T_{max} - c_{p_{min}} \rho_{min} V T_{min}} \tag{3}$$

Where c$_p$ is the specific heat capacity, ρ is the fluid density, V is the tank volume, T$_{max}$ is the maximum operating temperature, and T$_{min}$ is the minimum operating temperature.

The resulting RMSEs for temperatures and the SoC given in Table 9 show that the TTES model could reasonably simulate real conditions.

3.2. Results of the sensitivity study

Given in Fig. 11 are tornado plots that illustrate the sensitivity of the performance indicators to selected system parameters. These were generated by inducing a $\pm$ 5% change from the base value of each parameter and checking how they affect the SPF, LCOH, and GTC.

The figure shows that the SPF is most sensitive to the heat pump's high-side pressure and operating temperature, followed by the SH return temperature. The two most significant parameters for managing the SPF are operating parameters, which are controllable. Lowering the operating temperature and increasing the high-side pressure increased the SPF. However, there is a limit on how much change could be practically imposed on these parameters for improving the SPF. Typically, heat for

Table 8

Specifications of the ground thermal storage facility in Neckarsulm, Germany [76].

Parameter	Description
Working fluid	Water
Tube outer diameter, m	0.025 m
Tube inner diameter, m	0.0204 m
Tube shank spacing, m	0.065 m
Borehole depth, m	30 m
Borehole diameter, m	0.115 m
Borehole number	36
Borehole distance, m	2 m
Pipe thermal capacity, J/m^3-K	1.82×10^6
Pipe thermal conductivity, W/m-K	0.22
Grout thermal capacity,, J/m^3-K	3.58×10^6
Grout thermal conductivity, W/m-K	0.65
Ground thermal capacity, J/m^3-K	3×10^6
Ground thermal conductivity, W/m-K	2

Table 7

Results of the calibration CO$_2$ heat pump unit at ~60 °C Domestic Hot Water (DHW) temperature, ~35/30 °C supply /return temperature for space heating (data taken from [59]; Q$_{DHW}$ = Q$_{GC1}$ + Q$_{GC3}$; T$_E$ is the evaporator temperature in the CO$_2$ loop).

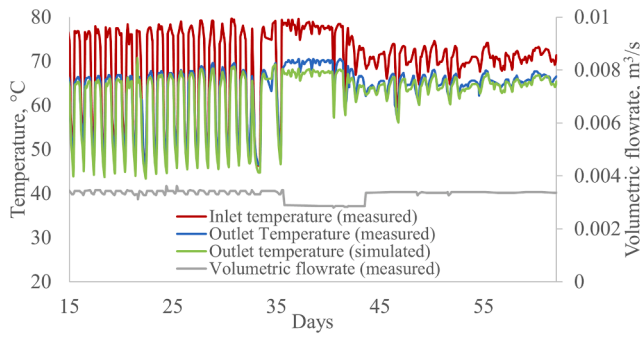| Data type	P$_{GC}$, bars	T$_E$, °C	Q$_{GC}$, W	Q$_{DHW}$, W	Q$_{GC1}$, W	Q$_{GC2}$, W	Q$_{GC3}$, W	Power$_C$, W	Tin/out$_{CO2\_GC}$, °C	M$_{CO2}$, kg/s	COP	Error
Measured*	85	−5.1	6907	3965	1608	2942	2357	1775	86.40/9.80	1.441	3.89	−0.26%
Calibrated	85	−5.1	6710	3776	1534	2934	2242	1730	86.56/9.80	1.449	3.88	
Measured*	89.8	−5	6947	4351	1550	2596	2801	1878	90.60/8.50	1.442	3.70	1.89%
Simulated	89.8	−5	6711	4074	1480	2637	2594	1779	90.76/8.17	1.417	3.77	
Measured	80.3	−5.1	6230	3502	1674	2728	1828	1699	81.60/18.00	1.440	3.67	4.90%
Simulated	80.3	−5.1	6595	3615	1707	2981	1907	1715	83.82/15.41	1.500	3.85	

*Design conditions.

Fig. 8. Comparison between measurement data and simulation output from MoBTES.
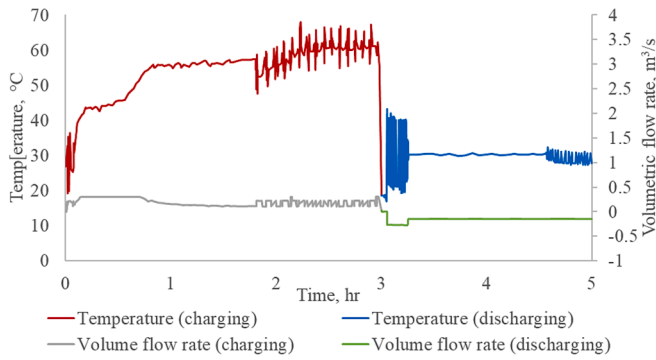

Fig. 9. Experimental flow and input temperature during charging and discharging, data taken from [77].

DHW heating should be greater than the proliferation temperature of Legionella bacteria (20–45 °C) [58]. Moreover, different distribution systems have different temperature requirements. Nonetheless, the trend now is to design these distribution systems so that it functions with

lower temperatures. As for the high-side pressure, it is well known that CO_2 heat pumps exhibit an optimal value due to the distinct working mode in the *trans*-critical region [22,78] so increasing the discharge pressure further will eventually lead to a lower SPF. Meanwhile, the SH return temperature is a parameter that cannot be easily managed since it is dependent on the design and efficiency of the distribution system. However, this is expected to be at least higher than the temperature required for thermal comfort. In the winter, this ranges from 15 to 21 °C [79].

The LCOH was seen to be most sensitive to the heat pump's high-side pressure and operating temperature. It was also notably reactive to the SH return temperature, the BHE length, and the SC area. This shows the importance of the cost of the operation, which is dependent on system efficiency. However, these results are dependent on the economic assumptions made. A higher discount rate can increase the importance of capital expenses, thereby increasing the influence of BHE length and SC area. A higher electricity cost can increase the contribution of the operations expenses. The BHE spacing could also possibly affect the LCOH. However, in this study, it was assumed that BHE cost is only associated with its length and not with the area it occupies.

The 1st year GTC was observed to be most reactive to the SC area and the BHE spacing. The heat pump's high-side pressure, operating temperature, and BHE length also significantly affected it. The SH return temperature and the mass flow rate of the fluid circulating through the SC and the BHE also affected the GTC, albeit to a lesser extent. The GTC is an indicator of the thermal imbalance in the ground induced by utilizing it for heating purposes. It is desired to maintain ground temperature near its initial state.

Among all the variables studied here, the heat pump's high-side pressure and output temperature are the most significant ones since they exhibited notable effects on all the performance indicators. Below the optimal operating pressure, a 5% increase in the heat pump's high-side pressure brought about a ~7–10% improvement to the SPF, a ~3–5% reduction to the LCOH, and a ~6–10% increase to the GTC. Reducing the output temperature by 5% increased the SPF by ~7–8%, decreased the LCOH by ~3%, and increased the GTC by ~6%. The parameter that did not significantly affect the performance indicators is
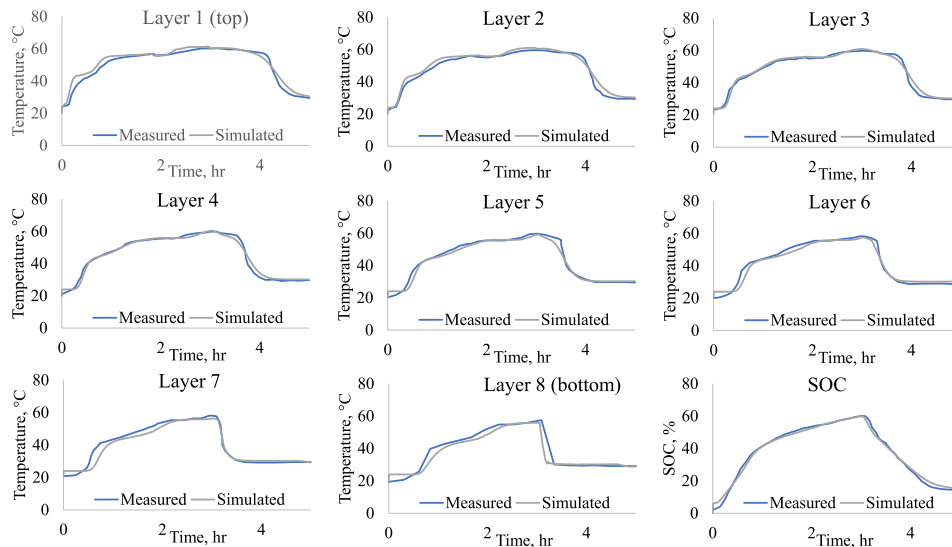

Fig. 10. Comparison of the measured and simulated temperatures in each layer of the TTES and its SoC, data taken from [77].

Table 9
RMSE of the TTES model for layer temperatures and SoC of the tank.

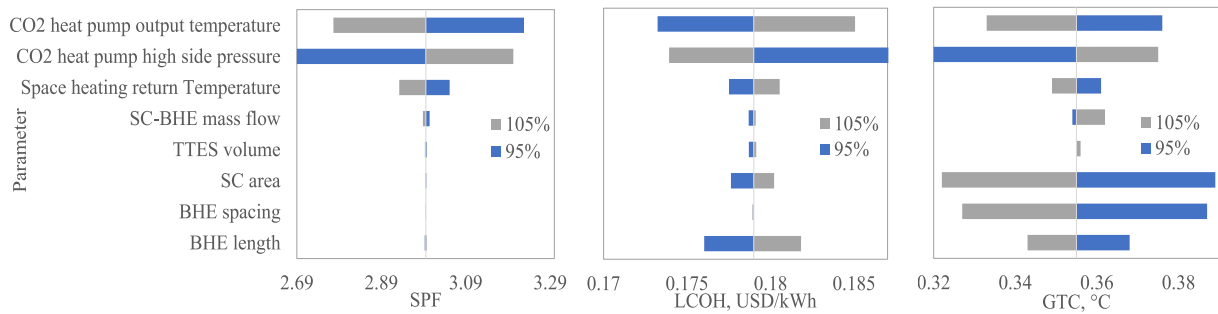| RMSE	Layer 1	Layer 2	Layer 3	Layer 4	Layer 5	Layer 6	Layer 7	Layer 8	SoC
	2.40	1.89	1.36	1.40	1.74	2.09	2.60	3.94	1.61

Fig. 11. Tornado plots showing the sensitivity of the performance indicators to different parameters.
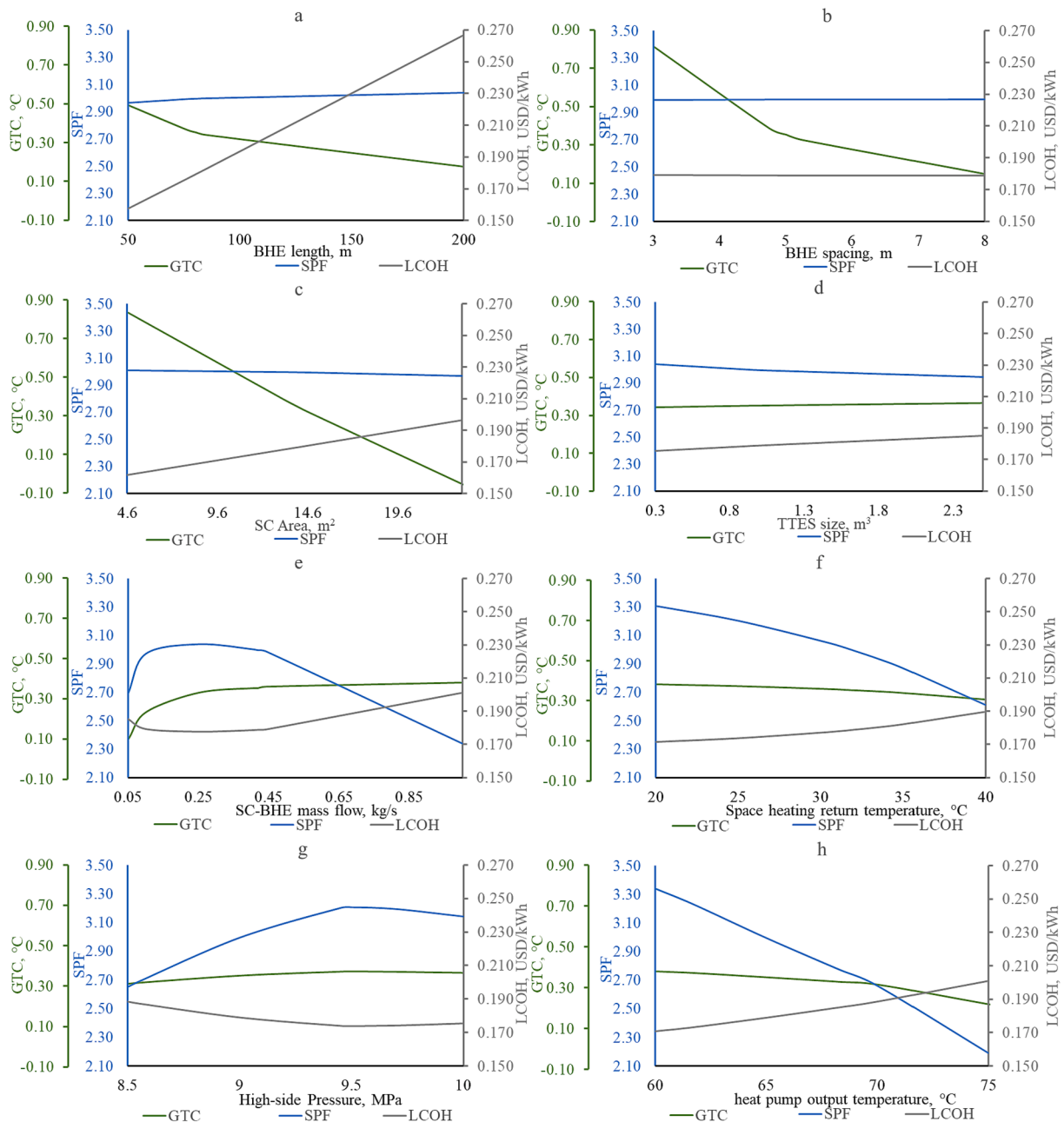

Fig. 12. Variation of SPF, LCOH, and GTC with different system parameters: (a) BHE length, (b) BHE space, (c) SC area, (d) TTES size, (e) SC-BHE mass flow, (f) SH return temperature, (g) Heat pump high-side pressure, and (h) heat pump output temperature.

the TTES volume.

3.3. Results of the parametric study

To see the effects of a wider range of parameter variation, their values were varied beyond the ± 5% limit set in the sensitivity analysis. The range implemented for each parameter is specified in Table 4. Given in Fig. 12 are the results of the parametric runs.

An optimal SPF was observed when the heat pump's high-side pressure was varied (Fig. 12g). Increasing the high-side pressure beyond 9.5 MPa decreased the SPF and increased the LCOH. The presence of an optimal discharge pressure can be explained by the trends of the isotherm lines in the supercritical region of CO_2. With the rise of the discharge pressure, the heating/cooling enthalpy difference increases substantially first and then only slightly, while the enthalpy difference from compression remains almost unchanged. At a relatively low discharge pressure, the heating/cooling COP increases as the discharge pressure increases because of the larger difference in the specific enthalpy between the state points in heat rejection/absorption relative to the enthalpy difference between the state points from compression. As the discharge pressure is further increased, the specific enthalpy difference between the heat rejection/absorption state points eventually gets smaller, resulting in a smaller COP. The larger heat absorption associated with the optimal point also explains the slightly higher GTC seen. A more illustrative explanation can be found in [78]. The LCOH also exhibited an optimal value, given that it is highly influenced by operational efficiency.

As for the SC-BHE mass flow rate (Fig. 12e), the SPF peaked at around 0.25 kg/s and then decreased sharply when the flow rate fell below 0.1 kg/s. When the circulation rate is lower, less heat is delivered to the heat pump, which causes the compressor to work harder to produce the necessary heat to maintain the same output temperature. This results in a lower SPF. Nonetheless, increasing the circulation rate increases electricity consumption for pumping. At some point, the benefits of higher heat delivery from a larger circulation rate are offset by the electricity consumption of the pump. This explains the presence of the optimal value of the SC-BHE mass flow rate that both maximizes the SPF and minimizes the LCOH. The GTC was seen to increase with the flow rate due to the larger heat extraction from a higher flow rate.

As discussed earlier, when the heat pump output temperature was decreased (Fig. 12h), the SPF and the LCOH improved. At a lower operating temperature, the heat pump was seen to (1) circulate a lower amount of CO_2, reducing compressor work, and (2) implement a larger change in specific enthalpy during the heat rejection process. It was also required to deliver a smaller amount of heat to maintain the lower output temperature. All of these contributed to better performance. However, this also resulted in a slightly larger amount of heat being extracted from the ground, given the larger specific enthalpy change during the heat absorption process. This caused the observed larger GTC.

Similarly, a lower SH return temperature implies a more efficient heat transfer to the distribution system (Fig. 12f). A higher SH return temperature involved the circulation of a larger amount of fluid to provide the heat needed by the distribution system. This required more pumping and a larger amount of heat from the heat pump, which both lowered the SPF. At times, the heat absorption process was also seen to occur at a lower temperature when the SH return temperature was lowered. This resulted in the slightly higher GTC seen in the plot.

The GTC changed more notably with BHE length (Fig. 12a), BHE spacing (Fig. 12b), and SC area (Fig. 12c). Increasing the values of these parameters resulted in lower GTCs. Temperature reduction in the ground should be minimized since it reduces the long-term efficiency of a GCHP system. Solar input offsets the thermal extraction induced by the system to the ground. Hence, increasing the SC area can reduce GTC and can even raise the ground temperature. However, it was also seen to slightly lower the SPF. A larger SC area increases the temperature of the

circulating fluid (propylene glycol–water mixture), which induces a small change to its density that slightly increases pump power consumption.

Increasing BHE spacing and length disperses ground heat extraction to a larger volume, thereby reducing its effects on ground temperature. BHE systems are typically oversized to reduce thermal imbalance [80]. However, oversizing them can be more expensive than adding SCs. Another less expensive way to offset the effects of heat extraction on the ground is to use the heat pump to extract heat from buildings and inject them into the ground. However, this may not be suitable for regions like western Norway where temperatures tend to remain quite low, even during the summer months. Increasing the SC area can increase ground temperature, which could eventually lead to a negative GTC. Increasing the BHE spacing and length would decrease GTC, but will not make it negative as long as the system is only being used for heating. A higher ground temperature might be good for use in heating, but inducing too much change could entail some unwanted environmental or ecological effects [81]. The best method to be used for managing the GTC will depend on the conditions in which the system will be used, such as area availability, ground temperature regulations, the presence of cooling demand, the intensity of solar irradiation, etc.

Increasing BHE length or SC area both entail costs so increasing the BHE spacing might be a better way to manage ground thermal imbalance. However, the relationship between BHE spacing and cost is artificially dissociated here. Increasing the spacing may also increase costs, but possibly to a much lesser extent than if the BHE length is increased.

Among all the parameters investigated, the TTES size exhibited the least effect on the performance indicators. Higher heat losses are expected to negatively affect system performance. However, in this work, heat losses from the tank to the ambient were minimized through insulation. Although higher TTES volumes resulted in greater heat losses due to the increased surface area, the impact on the SPF remained small. However, if a less insulated tank were used, changes to the TTES volume could potentially have a greater impact on performance.

The trade-offs of changing the values of the parameters when it comes to their effects on the performance indicators are shown by these plots. It is notable that changing the high-side pressure, the output temperature of the heat pump, and the SH return temperature to improve the SPF and LCOH could induce higher GTC. Hence, this should be accompanied by adjustments in other parameter values, such as increasing the BHE spacing or the SC area.

3.4. Long-term performance study

After observing how the CO_2 SAGCHP system reacted to the changes in various parameters, a combination of parameter values that are expected to give favorable overall performance was inferred and used for long-term simulation. The observed optimal high-side pressure of 9.5 MPa and SC-BHE mass flow rate of 0.25 kg/s were noted. Reducing the heat pump output set point temperature and the SH return temperature were seen to improve the SPF and LCOH so they were set to 60 °C and 25 °C (20 °C seems to be too low for most systems), respectively. The BHE length was maintained at the base value of 80 m, while the TTES size was kept at 1 m³. Increasing the BHE length can reduce GTC, but it is more cost-effective to increase the BHE spacing and the SC area to manage ground thermal imbalance. A well-insulated TTES was found to have a minimal effect on system performance, hence it was kept at its base value. Lastly, to eliminate ground temperature reduction, a BHE spacing of 8 m and an SC area of 23.2 m² (10 collectors) were used.

Shown in Fig. 13 are the SPF, LCOH, and GTC for the first 10 years of operating the system. The SPF and LCOH were calculated progressively. For example, the calculation of the 2nd year SPF was performed by taking into account the cumulative thermal energy generated and the total power used for the first two years of operations. As for the LCOH, it was calculated by assuming that annuities of the operations cost and energy generation are equivalent to the running annual average of the
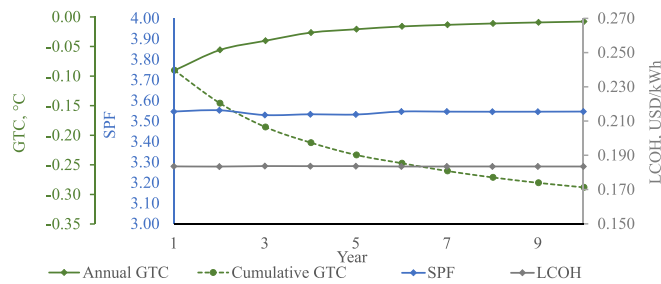
Fig. 13. Ten-year performance of the CO_2 SAGCHP system, assuming consistent demand.

operations cost and energy generation, i.e., for the 2nd year, it was calculated assuming that the average of the operation costs for the 1st and 2nd years is the annuity of the operations cost for its lifetime and the average of the energy generation for the 1st and 2nd years is the annual energy generation of the system throughout its lifetime. Two GTCs are shown here: (1) the annual GTC, which subtracts the average ground temperature from the temperature of the ground at the start of every year ($T_{\text{start of every year}} - T_{\text{end of every year}}$) and (2) the cumulative GTC, which subtracts the average ground temperature from the temperature of the ground prior to utilization ($T_{\text{start of the 1st year}} - T_{\text{end of every year}}$).

The SPF and LCOH did not vary so much. On the other hand, the absolute value of the annual GTC was seen highest in the first year and substantially decreased in the succeeding years. This behavior is also shown by the decreasing slope of the cumulative GTC curve. This was assuming that yearly demand levels are maintained.

The system exhibited an SPF of about 3.5, with slight variations that can be attributed to slight variations in the yearly weather conditions and ground temperature change. This value is comparable to the long-term performance of a conventional subcritical SAGCHP system used for SH and DHW heating ($\text{SPF}_{\text{conventional, SH}} = 3.89$; $\text{SPF}_{\text{conventional, SH+DHW}} = 3.17$ [82]; $\text{SPF} = 2.74$ to 3.27 [83]). However, these values from literature entail larger systems that apply different system configurations and boundary conditions. A better comparison could be obtained if a conventional SAGCHP model that applies identical conditions was used. Previous studies [54,82] have noted the importance of solar inputs in maintaining the performance of the system by showing the outputs from conventional SAGCHP and GCHP models. In our study, the SC induced a slight annual increase in ground temperature (a total of ~0.3 °C in 10 years), which helped in maintaining nearly consistent yearly SPFs. The temperature rise in the ground was seen to reduce substantially after the first year because the mean temperature difference between the ground and the circulating fluid gets lower every year. Larger variations in weather and demand can induce larger GTC variations. As for the LCOH, the value obtained here (0.183 USD/kWh) sits close to the upper bound of the range of conventional solar thermal combi heat pump systems LCOH (0.043 – 0.206 USD/kWh) [84]. This can be further lowered by finding the minimum BHE length and SC area that would still allow the system to consistently provide the required demand efficiently.

The simulation here was limited to only 10 years because of the relatively slow simulation speed, which could be attributed to the CO_2 heat pump component model. Alternative ways to model this component, such as the use of data-driven methods, should be explored. Nonetheless, with almost consistent demand and weather and with the GTC getting smaller, system performance is not expected to vary too much from what was shown here.

4. Conclusion

A Modelica model of a hybrid CO_2 SAGCHP system for SH and DHW heating was developed and used for investigating system performance by looking into three (3) performance indicators, namely, the SPF,

LCOH, and GTC. One-year simulation runs were implemented to perform the sensitivity and parametric studies. After that, a combination of parameter values that are expected to give favorable overall performance was inferred and used for long-term simulation. From these, the following were concluded:

- Without implementing component enhancements, like replacing the heat pump's throttle valve with an ejector, the CO_2 SAGCHP system is capable of reaching performances (SPF ~ 3.5) comparable to that of similar systems that use commercial working fluids operating at subcritical vapor compression cycle. This is possible by ensuring a good combination of design and operating specifications.
- The LCOH seen (0.183 USD/kWh) sits a bit closer to the upper bound of the range of conventional solar thermal combi heat pump systems' LCOH. To reduce this, optimization studies should be done to find the minimum BHE length and SC area that can provide the required demand while maintaining ground temperature for long-term utilization
- Among all the variables studied, the heat pump's high-side pressure and output temperature exhibited notable effects on all the performance indicators. Below the optimal operating pressure, a 5% increase in the heat pump's high-side pressure brought about a ~7–10% improvement to the SPF, a ~3–5% reduction to the LCOH, and a ~6–10% increase to the GTC. Reducing the output temperature by 5% increased the SPF by ~7–8%, decreased the LCOH by ~3%, and increased the GTC by ~6%. The heat pump's discharge pressure can be easily controlled using the throttle valve, but the output temperature is usually dictated by the heat distribution system
- The high-side heat pump pressure and SC-BHE circulation rate have optimal values that should be determined and used for operations
- Good insulation can minimize the effects of the TTES' volume on the overall performance
- Managing GTC ensures the longevity of the system. Practical ways to reduce ground temperature decline are by increasing BHE spacing, using the heat pump to cool spaces, or adding solar collectors. The best method depends on the condition in which the system would be used, such as area availability, ground temperature regulations, the presence of cooling demand, solar irradiation, etc.
- The model works, but the simulation time should be improved. This could be done by exploring alternative ways to model the CO_2 heat pump, such as by using data-driven methods

Declaration of Competing Interest

The authors declare that they have no known competing financial interests or personal relationships that could have appeared to influence the work reported in this paper.

Data availability

Data will be made available on request.

Acknowledgments

References

[1] European Commission, "Progress on competitiveness of clean energy technologies 4 & 5 - Solar PV and Heat pumps," Brussels, Oct. 2021. Accessed: Oct. 12, 2022. [Online]. Available: https://energy.ec.europa.eu/system/files/2021-10/swd2021_307_en_autre_document_travail_service_part3_v2.pdf.

[2] European Commission, "Eurostat," 2021. Accessed: Dec. 17, 2021. [Online]. Available: https://ec.europa.eu/eurostat/web/energy/overview.

[3] Wood Mackenzie, "Europe to install 45 million heat pumps in the residential sector by 2030." Aug. 04, 2022. Accessed: Oct. 12, 2022. [Online]. Available: https://www.woodmac.com/press-releases/europe-to-install-45-million-heat-pumps-in-the-residential-sector-by-2030/.

[4] Z. Weise, "EU looks at an electric alternative to Russian gas: The heat pump," POLITICO, Mar. 18, 2022. Accessed: Oct. 12, 2022. [Online]. Available: https://www.politico.eu/article/eu-heat-pumps-stop-russia-gas/.

[5] BSRIA Ltd., "BSRIA's view on refrigerant trends in AC and Heat Pump segments," Jan. 2020. Accessed: Nov. 14, 2022. [Online]. Available: https://www.bsria.com/uk/news/article/bsrias_view_on_refrigerant_trends_in_ac_and_heat_pump_segments/.

[6] K. Onno, "Report Annex 46 HPT-AN46-04: Refrigerants for Heat Pump Water Heaters," Heat Pump Centre c/o RISE – Research Institutes of Sweden, Borås, Dec. 2019. Accessed: Oct. 12, 2022. [Online]. Available: https://heatpumpingtechnologies.org/annex46/wp-content/uploads/sites/53/2020/10/hpt-an46-04-task-1-refrigerants-for-heat-pump-water-heaters-1.pdf.

[7] "EU legislation to control F-gases," Jan. 2015. Accessed: Apr. 01, 2022. [Online]. Available: https://ec.europa.eu/clima/eu-action/fluorinated-greenhouse-gases/eu-legislation-control-f-gases_en.

[8] United Nations, "The Kigali Amendment (2016): The amendment to the Montreal Protocol agreed by the Twenty-Eighth Meeting of the Parties (Kigali, 10-15 October 2016) | Ozone Secretariat," Oct. 2016. Accessed: Mar. 18, 2021. [Online]. Available: https://ozone.unep.org/treaties/montreal-protocol/amendments/kigali-amendment-2016-amendment-montreal-protocol-agreed.

[9] O. Bamigbetan, T.M. Eikevik, P. Nekså, M. Bantle, Review of vapour compression heat pumps for high temperature heating using natural working fluids, Int. J. Refrig 80 (Aug. 2017) 197–211, https://doi.org/10.1016/j.ijrefrig.2017.04.021.

[10] N. Abas, A.R. Kalair, N. Khan, A. Haider, Z. Saleem, M.S. Saleem, Natural and synthetic refrigerants, global warming: A review, Renew. Sustain. Energy Rev. 90 (Jul. 2018) 557–569, https://doi.org/10.1016/j.rser.2018.03.099.

[11] C. Chaichana, L. Aye, W.W.S. Charters, Natural working fluids for solar-boosted heat pumps, Int. J. Refrig. 26 (6) (Sep. 2003) 637–643, https://doi.org/10.1016/S0140-7007(03)00046-X.

[12] J. Wang, M. Belusko, M. Evans, M. Liu, C. Zhao, F. Bruno, A comprehensive review and analysis on CO2 heat pump water heaters, Energy Convers. Manage.: X 15 (Aug. 2022), 100277, https://doi.org/10.1016/j.ecmx.2022.100277.

[13] R.U. Rony, H. Yang, S. Krishnan, J. Song, Recent Advances in Transcritical CO2 (R744) Heat Pump System: A Review, Energies 12 (3) (2019), https://doi.org/10.3390/en12030457.

[14] Z. Jin, T.M. Eikevik, P. Nekså, A. Hafner, A steady and quasi-steady state analysis on the CO2 hybrid ground-coupled heat pumping system, Int. J. Refrig. 76 (Apr. 2017) 29–41, https://doi.org/10.1016/j.ijrefrig.2017.01.029.

[15] Navigant Consulting Inc., "Case Study: Transcritical Carbon Dioxide Supermarket Refrigeration Systems." Better Buildings Alliance - U.S. Department of Energy, Jan. 2015. Accessed: Oct. 12, 2022. [Online]. Available: https://betterbuildingssolutioncenter.energy.gov/sites/default/files/attachments/Transcritical_CO2_Supermarket_Refrigeration_Systems.pdf.

[16] G. Lorentzen, "Trans-critical vapour compression cycle device," WO1990007683A1, Jul. 12, 1990 Accessed: Feb. 17, 2021. [Online]. Available: https://patents.google.com/patent/WO1990007683A1/en.

[17] A. Hafner et al., "Efficient and integrated energy systems for supermarkets," 11th IIR Gustav Lorentzen Conference on Natural Refrigerants: Natural Refrigerants and Environmental Protection, GL 2014, pp. 311–319, Jan. 2014.

[18] Shecco, "World Guide to Transcritical CO2 Refrigeration," 2020. Accessed: Feb. 28, 2023. [Online]. Available: https://atmosphere.cool/fact_sheets/world-guide-to-transcritical-co2-refrigeration/.

[19] K. Hashimoto, Technology and Market Development of CO2 Heat Pump Water Heaters (ECO CUTE) in Japan, Accessed: Feb. 28, 2023. [Online]. Available: IEA Heat Pump Centre Newsletter (2006) http://waterheatertimer.org/pdf/Market-develop-CO2.pdf.

[20] AutomotiveTechinfo, "CO2 as a Refrigerant is Happening," Jun. 2021. Accessed: Feb. 28, 2023. [Online]. Available: https://automotivetechinfo.com/wp-content/uploads/2021/06/CO2-as-a-Refrigerant-is-Happening.pdf.

[21] M. Garry, "Volkswagen Offering CO2 Heat Pump for Electric Vehicles," Dec. 2020. Accessed: Feb. 28, 2023. [Online]. Available: https://accelerate24.news/regions/global/volkswagen-offering-co₂-heat-pump-for-electric-vehicles/2020/.

[22] Y. Song, C. Cui, X. Yin, F. Cao, Advanced development and application of transcritical CO2 refrigeration and heat pump technology—A review, Energy Rep. 8 (Nov. 2022) 7840–7869, https://doi.org/10.1016/j.egyr.2022.05.233.

[23] W. Kim, J. Choi, H. Cho, Performance analysis of hybrid solar-geothermal CO2 heat pump system for residential heating, Renew. Energy 50 (Feb. 2013) 596–604, https://doi.org/10.1016/j.renene.2012.07.020.

[24] N. Lawrence, S. Elbel, Theoretical and practical comparison of two-phase ejector refrigeration cycles including First and Second Law analysis, Int. J. Refrig. 36 (4) (Jun. 2013) 1220–1232, https://doi.org/10.1016/j.ijrefrig.2013.03.007.

[25] Z. Jin, A. Hafner, T.M. Eikevik, P. Nekså, Preliminary study on CO2 transcritical ejector enhanced compressor refrigeration system for independent space cooling and dehumidification, Int. J. Refrig. 100 (Apr. 2019) 13–20, https://doi.org/10.1016/j.ijrefrig.2019.01.027.

[26] A.F.A. Elbarghthi, V. Dvořák, Evaluation of Various Ejector Profiles on CO2 Transcritical Refrigeration System Performance, Entropy 24 (9) (2022), https://doi.org/10.3390/e24091173.

[27] A. Hafner, S. Försterling, K. Banasiak, Multi-ejector concept for R-744 supermarket refrigeration, Int. J. Refrig. 43 (Jul. 2014) 1–13, https://doi.org/10.1016/j.ijrefrig.2013.10.015.

[28] S. Fangtian, M. Yitai, Thermodynamic analysis of transcritical CO2 refrigeration cycle with an ejector, Appl. Therm. Eng. 31 (6) (May 2011) 1184–1189, https://doi.org/10.1016/j.applthermaleng.2010.12.018.

[29] S. Minetto, L. Cecchinato, R. Brignoli, S. Marinetti, A. Rossetti, Water-side reversible CO2 heat pump for residential application, Int. J. Refrig. 63 (Mar. 2016) 237–250, https://doi.org/10.1016/j.ijrefrig.2015.12.015.

[30] P. Gullo, A. Hafner, G. Cortella, Multi-ejector R744 booster refrigerating plant and air conditioning system integration – A theoretical evaluation of energy benefits for supermarket applications, Int. J. Refrig. 75 (Mar. 2017) 164–176, https://doi.org/10.1016/j.ijrefrig.2016.12.009.

[31] R.A. Otón-Martínez, F. Illán-Gómez, J.R. García-Cascales, F.J.S. Velasco, M. Reda Haddouche, Impact of an internal heat exchanger on a transcritical CO2 heat pump under optimal pressure conditions: Optimal-pressure performance of CO2 heat pump with IHX, Appl. Therm. Eng. 215 (Oct. 2022), 118991, https://doi.org/10.1016/j.applthermaleng.2022.118991.

[32] J.F. Ituna-Yudonago, J.M. Belman-Flores, F. Elizalde-Blancas, O. García-Valladares, Numerical investigation of CO2 behavior in the internal heat exchanger under variable boundary conditions of the transcritical refrigeration system, Appl. Therm. Eng. 115 (Mar. 2017) 1063–1078, https://doi.org/10.1016/j.applthermaleng.2017.01.042.

[33] J. Rigola, N. Ablanque, C.D. Pérez-Segarra, A. Oliva, Numerical simulation and experimental validation of internal heat exchanger influence on CO2 trans-critical cycle performance, Int. J. Refrig. 33 (4) (Jun. 2010) 664–674, https://doi.org/10.1016/j.ijrefrig.2009.12.030.

[34] Y.-J. Kim, K.-S. Chang, Development of a thermodynamic performance-analysis program for CO2 geothermal heat pump system, J. Ind. Eng. Chem. 19 (6) (Nov. 2013) 1827–1837, https://doi.org/10.1016/j.jiec.2013.02.028.

[35] F. Cao, Z. Ye, Y. Wang, Experimental investigation on the influence of internal heat exchanger in a transcritical CO2 heat pump water heater, Appl. Therm. Eng. 168 (Mar. 2020), 114855, https://doi.org/10.1016/j.applthermaleng.2019.114855.

[36] X. Qin, D. Wang, Z. Jin, J. Wang, G. Zhang, H. Li, A comprehensive investigation on the effect of internal heat exchanger based on a novel evaluation method in the transcritical CO2 heat pump system, Renew. Energy 178 (Nov. 2021) 574–586, https://doi.org/10.1016/j.renene.2021.06.082.

[37] IEA, "Heat Pumps," 2022. Accessed: Feb. 03, 2023. [Online]. Available: https://www.iea.org/reports/heat-pumps.

[38] Z. Han, C. Bai, X. Ma, B. Li, H. Hu, Study on the performance of solar-assisted transcritical CO2 heat pump system with phase change energy storage suitable for rural houses, Sol. Energy 174 (Nov. 2018) 45–54, https://doi.org/10.1016/j.solener.2018.09.001.

[39] S. Kumar, K. Murugesan, Optimization of geothermal interaction of a double U-tube borehole heat exchanger for space heating and cooling applications using Taguchi method and utility concept, Geothermics 83 (Jan. 2020), 101723, https://doi.org/10.1016/j.geothermics.2019.101723.

[40] H. Yang, P. Cui, Z. Fang, Vertical-borehole ground-coupled heat pumps: A review of models and systems, Appl. Energy 87 (1) (Jan. 2010) 16–27, https://doi.org/10.1016/j.apenergy.2009.04.038.

[41] W. Wu, H.M. Skye, J.J. Dyreby, Modeling and experiments for a CO2 ground-source heat pump with subcritical and transcritical operation, Energ. Conver. Manage. 243 (Sep. 2021), 114420, https://doi.org/10.1016/j.enconman.2021.114420.

[42] J. Wang, L. Kang, and J. Liu, "CO2 Transcritical Cycle for Ground Source Heat Pump," in 2009 WRI World Congress on Computer Science and Information Engineering, Mar. 2009, pp. 213–217. http://doi.org/10.1109/CSIE.2009.235.

[43] A. Bastani, P. Eslami-Nejad, M. Badache, A.T.A. Nguyen, Experimental characterization of a transcritical CO2 direct expansion ground source heat pump for heating applications, Energ. Build. 212 (Apr. 2020), 109828, https://doi.org/10.1016/j.enbuild.2020.109828.

[44] Z. Jin, T.M. Eikevik, P. Nekså, A. Hafner, Investigation on CO2 hybrid ground-coupled heat pumping system under warm climate, Int. J. Refrig. 62 (Oct. 2015) 145–152, https://doi.org/10.1016/j.ijrefrig.2015.10.005.

[45] Z. Jin, T.M. Eikevik, P. Nekså, A. Hafner, R. Wang, Annual energy performance of R744 and R410A heat pumping systems, Appl. Therm. Eng. 117 (May 2017) 568–576, https://doi.org/10.1016/j.applthermaleng.2017.02.072.

[46] J. Choi, B. Kang, H. Cho, Performance comparison between R22 and R744 solar-geothermal hybrid heat pumps according to heat source conditions, Renew. Energy 71 (Nov. 2014) 414–424, https://doi.org/10.1016/j.renene.2014.05.057.

[47] Dassault Systèmes, "Dymola," 2022. https://www.3ds.com/products-services/catia/products/dymola/ (accessed May 23, 2022).

[48] Claytex Technia Company, "Thermal Systems Library & TIL Suite." 2022. Accessed: May 23, 2022. [Online]. Available: https://www.claytex.com/products/dymola/model-libraries/thermal-systems-library/.

[49] J. Formhals, H. Hemmatabady, B. Welsch, D.O. Schulte, I. Sass, A Modelica Toolbox for the Simulation of Borehole Thermal Energy Storage Systems, Energies 13 (9) (2020), https://doi.org/10.3390/en13092327.

[50] Lawrence Berkeley National Laboratory, "Modelica Buildings library." Berkley, May 31, 2022. Accessed: Oct. 17, 2022. [Online]. Available: https://simulationresearch.lbl.gov/modelica/index.html.

[51] Q. Si, M. Okumiya, X. Zhang, Performance evaluation and optimization of a novel solar-ground source heat pump system, Energ. Build. 70 (Feb. 2014) 237–245, https://doi.org/10.1016/j.enbuild.2013.11.065.

[52] S.H. Razavi, R. Ahmadi, A. Zahedi, Modeling, simulation and dynamic control of solar assisted ground source heat pump to provide heating load and DHW, Appl. Therm. Eng. 129 (Jan. 2018) 127–144, https://doi.org/10.1016/j.applthermaleng.2017.10.003.

[53] L. Dai, S. Li, L. DuanMu, X. Li, Y. Shang, M. Dong, Experimental performance analysis of a solar assisted ground source heat pump system under different heating operation modes, Appl. Therm. Eng. 75 (Jan. 2015) 325–333, https://doi.org/10.1016/j.applthermaleng.2014.09.061.

[54] M. Lee, D. Lee, M.H. Park, Y.T. Kang, Y. Kim, Performance improvement of solar-assisted ground-source heat pumps with parallelly connected heat sources in heating-dominated areas, Energy 240 (Feb. 2022), 122807, https://doi.org/10.1016/j.energy.2021.122807.

[55] M. Lee, D. Cha, S. Yun, S.-M. Yoon, Y. Kim, Comparative heating performance evaluation of hybrid ground-source heat pumps using serial and parallel configurations with the application of ground heat exchanger, Energ. Conver. Manage. 229 (Feb. 2021), 113743, https://doi.org/10.1016/j.enconman.2020.113743.

[56] S.P. Kavanaugh, K.D. Rafferty, Geothermal Heating and Cooling: Design of Ground-source Heat Pump Systems, ASHRAE, 2014.

[57] ASHRAE, "EnergyPlus Weather Data (Bergen)." 2001. Accessed: Oct. 17, 2022. [Online]. Available: Deutsches Institut für Normung.

[58] Health and Safety Executive UK, "Managing legionella in hot and cold water systems," 2022. https://www.hse.gov.uk/healthservices/legionella.htm (accessed Nov. 14, 2022).

[59] J. Stene, "Residential CO2 Heat Pump System for Combined Space Heating and Hot Water Heating," Fakultet for ingeniørvitenskap og teknologi, 2004. Accessed: May 23, 2022. [Online]. Available: https://ntnuopen.ntnu.no/ntnu-xmlui/handle/11250/233381.

[60] J. Stene, Residential CO2 heat pump system for combined space heating and hot water heating, Int. J. Refrig. 28 (8) (Dec. 2005) 1259–1265, https://doi.org/10.1016/j.ijrefrig.2005.07.006.

[61] J. Formhals, "MoSDH - Modelica Solar District Heating library." Oct. 13, 2022. Accessed: Oct. 18, 2022. [Online]. Available: https://github.com/MoSDH/MoSDH.

[62] J. Formhals, "Object-oriented modelling of solar district heating grids with underground thermal energy storage," Ph.D. Thesis, Technische Universität Darmstadt, Darmstadt, 2022. doi: 10.26083/tuprints-00021506.

[63] J. Stene, "Ground-source heat pump systems in Norway IEA HPP Annex 29 (2004-2006)," Norway, NEI-NO–0706407, 2007. [Online]. Available: https://inis.iaea.org/search/search.aspx?orig_q=RN:38097084.

[64] K. Midttømme, Geothermal Energy in Norway and Hordaland [Online]. Available: Bergen Energy Lab (06 2017.) https://www.uib.no/en/energy/108628/kirsti-midtt%C3%B8mme-geothermal-energy-norway-and-hordaland.

[65] J.A. Duffie, W.A. Beckman, Solar Engineering of Thermal Processes, 4th ed., John Wiley & Sons Inc, New Jersey, 2013 [Online]. Available:.

[66] Deutsches Institut für Normung, "DIN EN 12975-1:2011-01 Thermal solar systems and components - Solar collectors - part 1: General requirements." Jan. 2011.

[67] TUV Rheinland DIN CERTCO, "DIN CERTCO - Registration Number 011-7S094 F: Summary of EN 12975 Test Results." 2014. Accessed: Oct. 18, 2022. [Online]. Available: https://www.dincertco.tuv.com/registrations/60064975?locale=en.

[68] Ø. Rønneseth, I. Sartori, Possibilities for Supplying Norwegian Apartment Blocks with 4th Generation District Heating, Accessed: Mar. 01, 2023. [Online]. Available: SINTEF akademisk forlag (2018) https://sintef.brage.unit.no/sintef-xmlui/handle/11250/2588923.

[69] R. Valančius, A. Jurelionis, R. Jonynas, V. Katinas, E. Perednis, Analysis of Medium-Scale Solar Thermal Systems and Their Potential in Lithuania, Energies 8 (6) (2015), https://doi.org/10.3390/en8065725.

[70] B. Badenes, M.Á. Mateo Pla, T. Magraner, J. Soriano, J.F. Urchueguía, Theoretical and Experimental Cost-Benefit Assessment of Borehole Heat Exchangers (BHEs) According to Working Fluid Flow Rate, Energies 13 (18) (2020), https://doi.org/10.3390/en13184925.

[71] F. Mauthner and S. Herkel, IEA SHC Task52 - Deliverable C1: Classification and benchmarking of solar thermal systems in urban environments. 2017. doi: 10.13140/RG.2.2.31437.28648.

[72] Y. Wang, S. Zong, Y. Song, F. Cao, Y. He, Q. Gao, Experimental and techno-economic analysis of transcritical CO2 heat pump water heater with fin-and-tube and microchannel heat exchanger, Appl. Therm. Eng. 199 (Nov. 2021), 117606, https://doi.org/10.1016/j.applthermaleng.2021.117606.

[73] C.J. Koroneos, E.A. Nanaki, Environmental impact assessment of a ground source heat pump system in Greece, Geothermics 65 (Jan. 2017) 1–9, https://doi.org/10.1016/j.geothermics.2016.08.005.

[74] Quintel, "Cost of capital | Energy Transition Model," 2023. https://docs.energytransitionmodel.com/main/cost-wacc/ (accessed Feb. 17, 2023).

[75] Statistics Norway, "09387: Electricity price, grid rent and taxes for households, by contents and quarter, accessed Feb. 17, 2023, Statbank Norway", SSB (2023), https://www.ssb.no/en/system/.

[76] D. Bauer, Zur thermischen Modellierung von Erdwärmesonden und Erdsonden-Wärmespeichern, University of Stuttgart, 2011 doctoralThesis,Accessed: Mar. 03, 2023. [Online]. Available:.

[77] I. De la Cruz-Loredo, et al., Experimental validation of a hybrid 1-D multi-node model of a hot water thermal energy storage tank, Appl. Energy 332 (Feb. 2023), 120556, https://doi.org/10.1016/j.apenergy.2022.120556.

[78] Y. Song, F. Cao, The evaluation of optimal discharge pressure in a water-precooler-based transcritical CO2 heat pump system, Appl. Therm. Eng. 131 (Feb. 2018) 8–18, https://doi.org/10.1016/j.applthermaleng.2017.11.092.

[79] N. Brelih, "Thermal and acoustic comfort requirements in European standards and national regulations," REHVA - Federation of European Heating, Ventilation, and Air Conditioning Associations, p. 4, Mar. 2013.

[80] T. Persson, O. Stavset, R.K. Ramstad, M.J. Alonso, K. Lorenz, Software for modelling and simulation of ground source heating and cooling systems, SINTEF Energy Research, Trondheim, Norway, TR A7570, 2016. Accessed: Feb. 17, 2021. [Online]. Available:.

[81] K. Zhu, L. Fang, N. Diao, Z. Fang, Potential underground environmental risk caused by GSHP systems, Procedia Eng. 205 (Jan. 2017) 1477–1483, https://doi.org/10.1016/j.proeng.2017.10.371.

[82] C. Xi, L. Lin, Y. Hongxing, Long term operation of a solar assisted ground coupled heat pump system for space heating and domestic hot water, Energ. Buildings 43 (8) (Aug. 2011) 1835–1844, https://doi.org/10.1016/j.enbuild.2011.03.033.

[83] G. Nouri, Y. Noorollahi, H. Yousefi, Solar assisted ground source heat pump systems – A review, Appl. Therm. Eng. 163 (Dec. 2019), 114351, https://doi.org/10.1016/j.applthermaleng.2019.114351.

[84] Iea, Levelized cost of heating (LCOH) for consumers, for selected space and water heating technologies and countries, accessed Feb. 23, 2023, IEA (2022), https://www.iea.org/data-and-statistics/charts/levelized-cost-of-heating-lcoh-for-consumers-for-selected-space-and-water-heating-technologies-and-countries.